On the optimum far-field irradiance distribution using Laguerre-Gaussian beams for intersatellite free-space optical communications

Badás, Mario; Piron, Pierre; Bouwmeester, Jasper; Loicq, Jérôme

DOI
10.1364/OE.533250

Publication date
2024

Document Version
Final published version

Published in
Optics Express

Citation (APA)
Badás, M., Piron, P., Bouwmeester, J., & Loicq, J. (2024). On the optimum far-field irradiance distribution using Laguerre-Gaussian beams for intersatellite free-space optical communications. *Optics Express*, *32*(18), 31597-31620. https://doi.org/10.1364/OE.533250

Important note
To cite this publication, please use the final published version (if applicable).
Please check the document version above.

Research Article | Vol. 32, No. 18 / 26 Aug 2024 / Optics Express 31597
Optics EXPRESS

On the optimum far-field irradiance distribution using Laguerre-Gaussian beams for intersatellite free-space optical communications

MARIO BADÁS,[1,*] PIERRE PIRON,[1] JASPER BOUWMEESTER,[1] AND JÉRÔME LOICQ[1,2]

[1]Department of Space Engineering, Delft University of Technology, Kluyverweg 1, 2629 HS Delft, Netherlands
[2]University of Liège, Centre Spatial de Liège, Avenue du Pré Aily, 4031 Liège, Belgium
[*]m.badasaldecocea@tudelft.nl

Abstract: This paper proposes a novel approach to improve the performance of free-space optical communication intersatellite links by combining fundamental Gaussian and higher-order Laguerre-Gaussian beams. We present a comprehensive mathematical model to analyze the system's performance, including received power statistics, average bit error probability, and outage probability. To generate the desired beam profiles, we propose an optical system capable of creating a superposition of orthogonally polarized Laguerre-Gaussian beams that yield the far-field irradiance distributions that optimize the communication performance. Our theoretical analysis demonstrates that the combination of fundamental Gaussian and higher-order modes can significantly enhance system performance compared to conventional fundamental Gaussian beams. In some scenarios, the proposed approach offers savings on the order of 20% to 40% of the required transmitted power.

1. Introduction

Free Space Optical Communications (FSOC) have been proposed as a key technology for the development of the future global communication networks. FSOC is based on sending laser beams to communicate information between two terminals. This technology provides higher data rates and more secure links than the current radiofrequency-based communications [1]. The first is due to the higher bandwidth available when higher frequencies are used for the carrier electromagnetic field. Furthermore, the higher security related to FSOC links is provided by the narrower beam at lower wavelengths, and also due to this technology being closely related to long-range free-space quantum communications [2–5].

Within the future global FSOC communication networks, intersatellite links play a key role. These links will enable long-distance, high data rate, and highly reliable communications [6–8]. Ground-based optical communication networks are limited by several factors. On the one hand, long-range fiber optics infrastructures are very costly and imply large power loss due to propagation through fibers [1]. On the other hand, in long-range terrestrial FSOC networks, light needs to travel large distances through atmospheric turbulence [9]. Considering the previous issues, intersatellite FSOC links can provide an alternative to the ground-based and radiofrequency-based communication technologies.

On an intersatellite link, the modulated laser is directed toward the receiver as accurately as possible. However, several perturbations occurring in the space environment will induce microvibrations of the satellite, e.g. reaction wheels, thermomechanical and gravitational effects [10]. All these sources combine to give rise to a stochastic pointing jitter that will deviate the

#533250 https://doi.org/10.1364/OE.533250
Journal © 2024 Received 18 Jun 2024; revised 23 Jul 2024; accepted 8 Aug 2024; published 15 Aug 2024

Optics EXPRESS

optical axis of the transmitter from the center of the receiver aperture (see Fig. 1). The effect of this stochastic process is a fluctuation in the power collected by the receiver aperture that is detrimental to the communication performance. The high directivity of narrow laser beams can only be exploited if the transmitter pointing jitter is maintained within some operational range. In fact, the divergence of the laser beams needs to be adjusted for the amount of pointing jitter that is expected in the transmitter terminal.

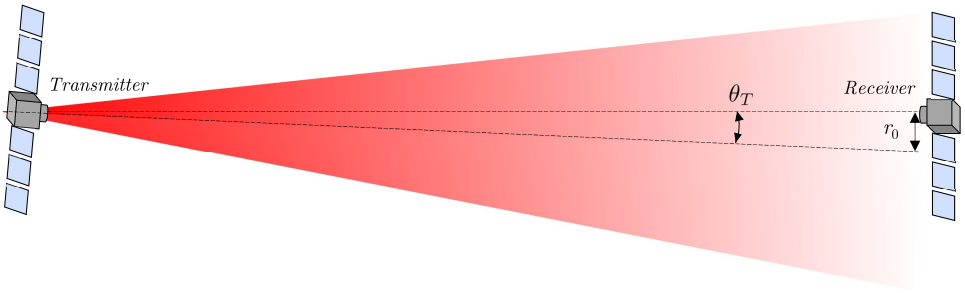

Fig. 1. Transmitter pointing error given by an angle θ_T for an intersatellite link.

The effect of this power reduction on the communication performance of the link has been thoroughly studied in the past. Most of the work available in the literature combines the atmospheric and the pointing jitter effects [11–13], although some of them consider the intersatellite link scenario in which only the pointing jitter plays a role [14–17]. Some of these papers not only present models to compute the effect of the pointing jitter but also optimize the link performance considering the detrimental effect of the pointing jitter. There are several approaches to optimize the link performance by varying different parameters and maximizing (or minimizing) different objective functions. Most of them consist of varying the beam divergence of the transmitted beam to minimize Average Bit Error Probability (ABEP) [15,16,18] or the outage probability [11]. Furthermore, research has also been done on the receiver architectures and the modulation techniques used to communicate [17,19]. On the other hand, a huge effort is being devoted to reducing the microvibrations on board satellites to reduce the pointing jitter of FSOC terminals in space [20].

However, all the research done so far, to the best of the knowledge of the authors, has been done considering a Gaussian beam as seen by the receiver aperture plane. However, under the effect of the transmitter pointing jitter, the Gaussian irradiance distribution might not be the optimum for the communication performance on an intersatellite link. In this paper, we propose to use a superposition of linearly orthogonally polarized higher-order Laguerre-Gaussian beams to improve the communication performance on intersatellite FSOC links. It is investigated if these beams can improve the communication performance on intersatellite links and how they can be generated onboard an FSOC terminal.

Firstly, the model to compute the statistics of the received power is presented for a given irradiance distribution on the receiver aperture (Section 2.1). Secondly, the model to compute several communication performance parameters from the received power statistics is presented in Section 2.2. An optical system to generate these beams is also proposed explaining the limitations of such a system and the design decisions made (Section 3). Finally, the numerical results showing the optimum far-field distributions are presented, demonstrating an improvement in performance due to the beams proposed by the authors.

Optics EXPRESS

2. Received power statistics and communication performance

The high directionality of the laser beam in an FSOC link enables lower free space power losses, meaning that compared to a less directional beam more power will reach the receiver's aperture. However, this directionality can only be exploited up to a certain point due to the transmitter pointing jitter. For the satellite-based links studied in this work, this pointing jitter is due to micro-vibrations of the platform that originate in the orbit environment. The magnitude of the pointing jitter has been measured in several optical and quantum communication satellites and ranges from sub-microradians to milliradians [10]. Although the deviation of the beam due to the microvibrations can be reduced with coarse and fine pointing assembly mechanisms (e.g., gimbals and fast steering mirrors), the pointing jitter in the transmitter terminal onboard a satellite will always occur to a higher or lower extent. The transmitter pointing error deviates the center of the beam from the optical axis of the receiver. For a Gaussian beam, as the maximum power is concentrated in the center of the beam, this mispointing diminishes the power collected by the aperture of the receiver. Finally, these power fluctuations deteriorate the performance of the optical communication link. Hence, it is very important to correctly model and understand the magnitude of these power fluctuations and how they affect the communication performance of the system. In this section, the model to compute the received power statistics is presented for a given far-field distribution and different pointing jitter models. Furthermore, the equations to evaluate the communication performance parameter for a Probability Density Function (PDF) of the received power in different scenarios are presented.

2.1. Received power statistics

The power received will vary over time as the transmitter pointing error changes due to jitter (see Fig. 2). Hence, the received power can be characterized statistically by a PDF [13,21]. In doing so, the temporal information of the power fluctuations is lost. However, as the received power variations due to the pointing jitter are orders of magnitude slower than the modulation period of the communication signal (the power fluctuations due to the pointing jitter will be below kHz while the modulation will be at least in the MHz domain), the slow-fading channel model can be considered for the intersatellite link [11]. Therefore, as many bits of information are affected by the power variation due to a certain pointing error, the power fluctuations can be characterized by a PDF. More detail on the slow-fading channel is presented in Section 2.2. In this section, the equations to compute the PDF of the received power are presented. Firstly, the most general situation is explained in which no assumptions of the irradiance field (at the receiver aperture plane) and statistics of the pointing jitter are made. Figure 3 illustrates the whole process for obtaining the normalized received power PDF from a far-field irradiance and the pointing error PDF, the received power P is normalized by the transmitter power P_t, resulting in the normalized received optical power $h = P/P_t$.

The power captured by the receiver aperture for a given pointing error can be computed by integrating the irradiance field across the aperture. Using a Cartesian coordinate system as shown in Fig. 2, the power received as a function of the displacement of the center of the beam is

$$g'(x_0, y_0) = \iint_{\mathbb{R}^2} I(x - x_0, y - y_0)\, \mathcal{A}(x, y)\, dxdy \tag{1}$$

where $I(x, y)$ is the expression for the centered irradiance field (see Fig. 3(a)) and $\mathcal{A}(x, y)$ is the pupil function of the receiver aperture given by

$$\mathcal{A}(x, y) = \begin{cases} 1 & \text{if} \quad a \leq \sqrt{x^2 + y^2} \leq b \\ 0 & \text{else} \end{cases} \tag{2}$$

where a is the radius of the obscuration due to the secondary mirror and b is the radius of the primary mirror of the telescope (see Fig. 2). For the sake of completeness, the most general case

Optics EXPRESS

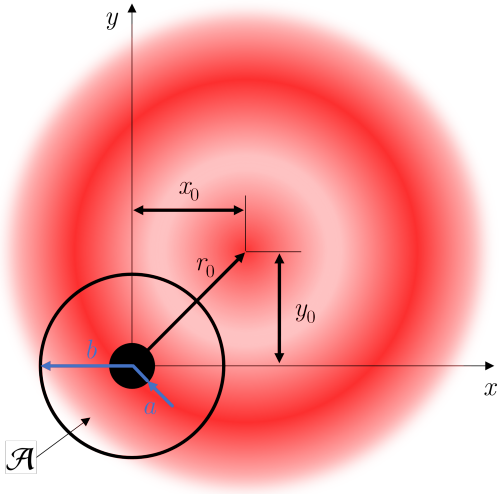

Fig. 2. Generic far-field irradiance distribution in the receiver's aperture plane for a decentered beam. a and b are the inner and outer radius of the aperture and r_0 is the instantaneous pointing error in meters.

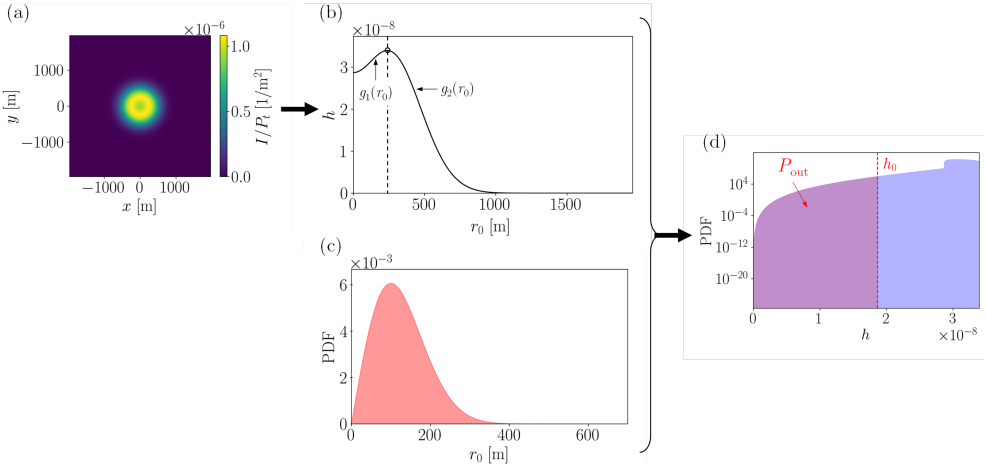

Fig. 3. Process followed to obtain the received power statistics and the communication performance parameters for $LG_{00} + LG_{10}$ with $a_0 = 0.345$, $a_1 = 0.655$, $w_z/\sigma = 4.903$, $\sigma = 100$ m, $P_t = 25$ dBm, and the rest of the parameters given in Table 1. a_0 and a_1 are the contributions of the fundamental and the higher-order Laguerre-Gaussian modes to the total power, see Eq. (15). (a) Far-field irradiance distribution at the receiver, (b) normalized received power as a function of the pointing error, (c) PDF of the pointing error, and (d) PDF of the normalized received power.

Optics EXPRESS

Table 1. Parameters used for the numerical simulations.

Parameter	Symbol	Value	Remarks
Noise standard deviation	$\sigma_n^2 = N_0 R_0 / R_{load}$	4.7×10^{-9} A	[11]
Noise power spectral density	N_0	−174 dBm/Hz	[16]
Receiver load resistance	R_{load}	179700 Ω	[18]
Receiver aperture diameter	$2b$	20 cm	
Pointing jitter standard deviation	σ	10, 100, 1000 m	
Carrier wavelength	λ	1550 nm	
Responsivity	$R = e\eta/h\nu$	0.8153 A/W	[16]
Data rate	R_0	1 Gbps	
Rate	D_0	0.5 bits/channel use	
Average Transmitter power	P_t	$\in (0, 50)$ dBm	

for a receiver aperture obscured by an on-axis secondary mirror is presented here. However, by setting the inner radius $a = 0$, the case of the clear aperture would be obtained (i.e. off-axis secondary mirror or refractive telescopes). According to Eq. (1), the power received is a bi-dimensional convolution of the irradiance field $I(x, y)$ and the pupil function $\mathcal{A}(x, y)$. Then, the received power can be computed using the convolution theorem as

$$g'(x_0, y_0) = \{I * \mathcal{A}\}(x_0, y_0) = \mathcal{F}^{-1}\{\mathcal{F}(I) \cdot \mathcal{F}(\mathcal{A})\} \tag{3}$$

where $\mathcal{F}$ and $\mathcal{F}^{-1}$ are the bidimensional direct and inverse Fourier transforms, respectively. The bidimensional Fourier transforms involved in this calculation, can be numerically evaluated efficiently using the Fast Fourier Transform. Finally, the expression of the power as a function of the displacement of the center of the beam w.r.t the optical axis of the receiver, $g'(x_0, y_0)$, can be combined with the PDF of the displacement of the beam center to obtain the PDF of the received power. In general, the PDF of the pointing jitter, and therefore of the displacement of the beam center from the receiver's optical axis, will be axially symmetric with respect to the optical axis of the receiver. Given that the PDF of the pointing jitter is axially symmetric and that the aperture of the receiver is also considered axially symmetric w.r.t. the same axis, the irradiance distributions that will be investigated throughout this paper will keep this symmetry. Therefore, the irradiance distributions on the far-field will also be considered axially symmetric. Under these considerations, the power collected as a function of the displacement of the center of the beam will maintain this symmetry and can be expressed as (see Fig. 3(b))

$$P = g'(x_0, y_0) = g\left(\sqrt{x_0^2 + y_0^2}\right) = g(r_0) \tag{4}$$

where r_0 is the radial displacement of the center of the beam due to the transmitter pointing jitter. Finally, to obtain the PDF of the received power, given a PDF of the radial pointing jitter $f_R(r_0)$ (see Fig. 3(c)), in general, the expression for a non-monotonic function $g(r_0)$ will be considered. In the Gaussian beam case, the function $g(r_0)$ will be monotonic and this conversion will be more simple. However, for the far-field irradiance patterns given by the orthogonally polarized superposition of Laguerre-Gaussian beams proposed in this work, the function $g(r_0)$ can be non-monotonic. To obtain the PDF of a given scalar variable (the received power P) from the PDF of another variable (the pointing error r_0), given that these variables are interdependent, the general expression for a non-monotonic $g(r_0)$ function is (see Ref. [22], Eq. 7.2-23)

$$f_{\mathcal{P}}(P) = \sum_{k=1}^{n(P)} \left| \frac{d}{dP} g_k^{-1}(P) \right| \cdot f_R\left(g_k^{-1}(P)\right) \tag{5}$$

Optics EXPRESS

where $f_{\mathcal{P}}(P)$ is the PDF of the received power, and $n(P)$ is the number of intervals between successive maxima and minima values of the function $g(r_0)$. $g_k^{-1}(P)$ is the kth inverse function of $g(r_0)$ in each of these intervals (see example in Figs. 3(b) and 3(c), where the index k takes values $1, 2$).

The general expressions for obtaining the PDF of the received power have been derived (Eqs. (1)–(5)), under the only assumption that the problem is axially symmetric. In the following, different assumptions and considerations are made and some analytical approximations are obtained for each of these.

2.1.1. Gaussian beam

First of all, a Gaussian beam will be considered. Hence, the pattern in the far-field irradiance will be Gaussian and can be written as

$$I_G(r,z) = I_0 \left(\frac{w_0}{w(z)}\right)^2 \exp\left(-\frac{2r^2}{w(z)^2}\right) \qquad w(z) = w_0 \sqrt{1 + \left(\frac{z}{z_R}\right)^2} \tag{6}$$

where I_0 is the irradiance at the center of the beam, w_0 is the beamwaist, r is the radial coordinate, z is the distance from the beamwaist location along the propagation axis of the beam and $z_R = \pi w_0^2 n/\lambda$ is the Rayleigh range. The main body of research done in FSOC has focused on these types of beams for several reasons. First of all, Gaussian beams can be generated by most of the commercially available laser sources, as they are the fundamental mode of a laser cavity. Furthermore, the Gaussian beam is the fundamental beam mode of the single-mode optical fibers that are frequently used in free-space optical communication terminals, i.e. optical amplification in the transmitter side [23]. Finally, the irradiance profile of the main lobe of the diffraction pattern due to the clipping of the transmitter aperture can be fairly approximated to a Gaussian irradiance profile [24].

Regarding the PDF of the angular pointing jitter, this is usually considered to be given by a Rayleigh distribution. The Rayleigh distribution is the result of the combination of independent centered normal PDFs in both elevation and azimuth angles with the same standard deviations [15]. For the small angle approximation (up to $\sim$ 100 mrad), it can be proven that the angular Rayleigh distribution is converted into a radial Rayleigh distribution of the displacement of the center of the beam r_0 in the receiver's aperture plane (see Supplement 1). Due to the stochastic nature of the pointing jitter and its multi-variable origin, the normal PDF in both elevation and azimuth angles is justified by the central limit theorem. Furthermore, the in-orbit experimental measurements of the micro-vibrations of different optical and quantum communication satellites have shown to have this type of angular pointing jitter PDFs [25–27]. The Rayleigh PDF of the displacement of the center of the beam, r_0, is written as

$$f_R(r_0) = \frac{r_0}{\sigma^2} \exp\left(-\frac{r_0^2}{2\sigma^2}\right) \tag{7}$$

where σ is the scale parameter and is the same as the standard deviation of the underlying normal distributions in x and y axes. The scale parameter is related to the scale parameter of the angular pointing jitter σ_θ by $\sigma = \sigma_\theta z$, being z the distance from the center of the transmitter to the center of the receiver (small angle approximation).

Considering a Gausssian beam under a pointing jitter given by a Rayleigh distribution, Eqs. (1)–(5) can be combined with Eqs. (6) and (7) to find the following approximation of the received power [11]

$$f_{\mathcal{P}}(h) = \frac{\gamma_1^2}{B_0^{\gamma_1^2}} h^{\gamma_1^2 - 1} \qquad 0 \le h \le B_0 \tag{8}$$

Optics EXPRESS

$$B_0 = [\mathrm{erf}(v)]^2 \qquad v_b = \frac{\sqrt{\pi}b}{\sqrt{2}w_z} \qquad \gamma_1 = \frac{w_{\mathrm{eq},1}}{2\sigma} \qquad w_{\mathrm{eq},1}^2 = w_z^2 \frac{\sqrt{\pi}\mathrm{erf}(v_b)}{2v_b \exp\left(-v_b^2\right)}$$

where $h = P/P_t$ is the received power normalized by the transmitted power, b is the radius of the receiver aperture, and $w_z = w(z)$ has been written to simplify the notation. This approximation is obtained by approximating the circular aperture (without the secondary mirror obscuration) to a squared aperture of the same area and expanding the integral of the received power Eq. (1) in Taylor series. This approximation gives a normalized mean squared error smaller than 10^{-3} for $w(z)/b$ bigger than six [11]. However, when bigger apertures are needed in the receiver terminal, on-axis secondary mirrors are usually used for reflective telescopes in satellite communication terminals [28,29]. Although off-axis telescope configurations can also be considered, they have several drawbacks such as more complex alignment or maximum field of view. Furthermore, due to the higher angles of incidence of the light impinging the mirrors in off-axis configurations the effects on the polarization have to be taken care of [30]. Therefore, an expression for the PDF of the received power has to be considered when there is an obscuration due to a secondary mirror. By approximating the secondary mirror obscuration area by an equivalent squared section with the same area, a more general approximation can be obtained (see Supplement 1)

$$f_{\mathcal{P}}(h) = \frac{\gamma_2^2}{C^{\gamma_2^2}} h^{\gamma_2^2-1} \qquad 0 \le h \le C \tag{9}$$

$$C = B_0 - A_0 \qquad A_0 = [\mathrm{erf}(v_a)]^2 \qquad v_a = \frac{\sqrt{\pi}a}{\sqrt{2}w_z} \qquad \gamma_2 = \frac{w_{\mathrm{eq},2}}{2\sigma} \qquad w_{\mathrm{eq},2}^2 = \left|\frac{A_0 - B_0}{B_2 - A_2}\right| w_z^2$$

$$A_2 = -\frac{2}{\sqrt{\pi}}\mathrm{erf}(v_a)\left[v_a\ \mathrm{erf}(-v_a^2)\right] \qquad B_2 = -\frac{2}{\sqrt{\pi}}\mathrm{erf}(v_b)\left[v_b\ \mathrm{erf}(-v_b^2)\right]$$

where B_0 and v_b are defined in Eq. (8). The Rayleigh distribution considered for characterizing the pointing jitter, is a special case of the more general Rice distribution. The Rice distribution has also been considered to model the pointing jitter when considering non-zero mean normal distributions in both elevation and azimuth angles [13]. This non-zero mean is referred to as boresight error in optical communications and can be due to several factors. For an intersatellite link, it is usually considered that the pointing jitter has a negligible boresight error because optical axis calibration of the transmitted beam is carried out periodically [15]. However, wavefront aberrations could induce misalignment between the transmitted beam path and the received beacon paths, which could cause a systematic bias in pointing jitter [31]. Therefore, for the sake of completeness, the non-zero boresighted PDF of the pointing jitter, i.e., the Rice probability distribution [32], is also considered in this work. The Rice distribution is given by

$$f_R(r_0) = \frac{r_0}{\sigma^2} \exp\left[\frac{-(r_0^2 + s^2)}{2\sigma^2}\right] \mathcal{J}_0\left(\frac{r_0\, s}{\sigma^2}\right) \tag{10}$$

where σ is the scale parameter, $\mathcal{J}_0$ is the zeroth order modified Bessel function of the first kind, and s is the boresight error. For a Gaussian beam under a transmitter pointing jitter characterized by a Rice PDF, the PDF of the power for a circular aperture can be approximated as [13]

$$f_{\mathcal{P}}(h) = \frac{\gamma_1^2 \exp\left(\frac{-s^2}{2\sigma^2}\right)}{B_0^{\gamma_1^2}} h^{\gamma_1^2-1} \mathcal{J}_0\left(\frac{s^2}{\sigma^2}\sqrt{\frac{-w_{\mathrm{eq},1} \ln \frac{h}{B_0}}{2}}\right) \qquad 0 \le h \le B_0 \tag{11}$$

where the terms are defined in Eq. (8). Following the same process as for the Rayleigh distribution, this PDF can be generalized to the case in which there is an obscuration due to the secondary

Optics EXPRESS

mirror to

$$f_{\mathcal{P}}(h) = \frac{\gamma_2^2 \exp\left(\frac{-s^2}{2\sigma^2}\right)}{C^{\gamma_2^2}} h^{\gamma_2^2-1} \mathcal{J}_0\left(\frac{s^2}{\sigma^2}\sqrt{\frac{-w_{\mathrm{eq},2}\ln\frac{h}{C}}{2}}\right) \qquad 0 \le h \le C \tag{12}$$

where the terms are defined in Eqs. (8) and (9). When the aperture of the receiver is much smaller than the beamwidth $w(z)>>b$, then it can be shown (see Supplement 1 for the proof) that under a Rayleigh PDF of the transmitter pointing jitter the PDF of the received power can be modeled as a beta distribution

$$f_{\mathcal{P}}(h') = \left(\frac{\pi w_z^2}{2A^2}\right)^{\beta-1} \beta\, h'^{\beta-1} \qquad 0 \le h' \le \frac{2A^2}{\pi w_z^2 P_t} \tag{13}$$

where $\beta = w_z^2/(4\sigma^2)$, A is the area of the receiver aperture, $h' = P/I_{0,z}A$ and $I_{0,z}$ is the irradiance at the center of the Gaussian beam in the receiver aperture plane. In this case, both expressions for the clear aperture telescope and on-axis secondary mirror configurations will be the same, as only the area of the aperture is involved and the variation of the irradiance across the aperture of the receiver is completely neglected.

From the expressions above, it can be seen that the PDF of the received power can be varied by changing the beamwidth of the Gaussian beam in the receiver aperture plane $w(z)$. This is equivalent to changing the divergence of the Gaussian beam, and the approach has been thoroughly investigated in the literature [11,18,33]. The divergence of the Gaussian beam is adjusted by properly designing the optical relay on the transmitter side to adjust its underlying beamwaist w_0 in Eq. (6). Furthermore, dynamic beam divergence adjustment methods have also been proposed to adjust the divergence [34]. Indeed, an intuitive explanation can be found for the existence of an optimum beamwidth in the far field to optimize the power received: when the beamwidth is very small compared to the aperture of the receiver, it will be very sensitive to the pointing error and the signal will be completely lost when the beam center is slightly displaced. This effect can be compensated by increasing the beamwidth, however, maintaining the transmitted power constant, for large beamwidths the power collected by the receiver aperture will be very low. Hence, an optimum point will exist somewhere in between these two extremes given a pointing jitter and a receiver aperture. The optimum received power PDF for communication performance will be discussed in the next section.

2.1.2. Orthogonally polarized Laguerre-Gaussian beams

In this paper, the use of higher-order Laguerre-Gaussian beams is proposed to change the far-field irradiance distribution. This new degree of freedom (added to the far field beamwidth) will allow us to further change the received power PDF to increase the performance of intersatellite communication links. The far-field irradiance distribution obtained when non-interfering higher-order Laguerre-Gaussian modes are considered is (a way of achieving the non-interference condition is presented in Section 3)

$$I(r,z) = \frac{1}{2\eta_0}\sum_l \left(a_l \left|U_{lp}(r,\phi,z)\right|^2\right) \tag{14}$$

where $\eta_0 = 377\ \Omega$ is the wave impedance of free space, a_l are the weighting coefficients for each azimuthal mode superposed, and U_{lp} is the complex electromagnetic field of the Laguerre-Gaussian mode with radial index $p \ge 0$ and azimuthal index l. When the radial index is set to

Optics EXPRESS

$p = 0$, and only the fundamental Gaussian mode and a higher-order Laguerre-Gaussian mode are considered (as will be done in this work), the far-field irradiance expression above simplifies to

$$I(r,z) = \frac{1}{2\eta_0}\left(a_0\,|U_{00}(r,\phi,z)|^2 + a_l\,|U_{l0}(r,\phi,z)|^2\right) \tag{15}$$

where l is the azimuthal order of the higher-order Laguerre-Gaussian mode considered. Considering the $a_0 + a_l = 1$, the final irradiance field is normalized to the power unit. The complex electromagnetic field for each Laguerre-Gaussian mode is given by

$$\begin{aligned} U_{lp}(r,\phi,z) = C_{lp}\frac{1}{w(z)}\left(\frac{r\sqrt{2}}{w(z)}\right)^{|l|}\exp\left(-\frac{r^2}{w^2(z)}\right)L_p^{|l|}\left(\frac{2r^2}{w^2(z)}\right)\times \\ \exp\left[-i\left(k\frac{r^2}{2R(z)} + l\phi - \psi(z)\right)\right] \end{aligned} \tag{16}$$

where

$$R(z) = z\left[1 + \left(\frac{z_{\mathrm{R}}}{z}\right)^2\right] \tag{17}$$

$$\psi(z) = (|l| + 2p + 1)\,\arctan\left(\frac{z}{z_{\mathrm{R}}}\right) \tag{18}$$

$$C_{lp} = \sqrt{\frac{2p!}{\pi(p+|l|)!}} \tag{19}$$

being $\psi(z)$ the Gouy phase, C_{lp} a normalization constant and $L_p^{|l|}$ the generalized Laguerre polynomials. The Laguerre-Gaussian modes are the solution to the scalar paraxial Helmholtz equation in polar coordinates [35]. The complex scalar field of these beams generates an orthonormal basis. Furthermore, these beams have an orbital momentum of light associated with the azimuthal order l. The orbital angular momentum of light has been widely investigated to increase the capacity of free-space optical communication links by mode division multiplexing [36–39]. The application of this division multiplexing technique is limited to short-range free-space optical links because the beam has to be fully contained within the aperture of the receiver to demultiplex the signal [40,41]. However, the scope of this paper is to use higher-order Laguerre-Gaussian modes along with the fundamental Gaussian beam, to change the irradiance distribution on the far field for intersatellite free-space optical communications. Laguerre-Gaussian beams have been considered to solve the problem because of their symmetry around the optical axis in their irradiance fields. As it has been mentioned before, the pointing jitter in free-space optical communications is symmetric to the optical axis and hence the solution to it will also keep this property. Furthermore, these beams have already been used for other applications in free-space optical communications, such as multiplexing and noise mitigation [42], and their behavior under atmospheric turbulence has also been investigated [43]. Hence, the research presented in this paper can be expanded to FSOC links through atmospheric turbulence (the irradiance fields on the receiver aperture would need to be computed to account for the speckle patterns generated during the propagation through turbulence). As it will be explained later, the generation of these beams can be accomplished with a simple optical setup and therefore implemented on satellite optical communication terminals.

Other types of beams have also been proposed for their application in FSOC links, such as Airy beams [44,45], Bessel beams [46–48], bottle vortex beams [49] and Hermite-Gaussian beams [50,51]. However, the use of these types of beams has been limited to (1) increasing the capacity of the channel through multiplexing, (2) avoiding obstructions in the link and (3) mitigating the atmospheric turbulence effects. By contrast, in the present paper, the authors propose the combination of higher-order Laguerre-Gaussian beams to mitigate the detrimental impact of the

Optics EXPRESS

transmitter pointing error by tuning the far-field irradiance distribution in the receiver's aperture plane. However, although it is out of the scope of the present paper, the application of some of the mentioned beams for creating optimum far-field irradiance fields should be investigated further.

Some Laguerre-Gaussian modes are presented in Fig. 4. In this figure, only the radial order $p = 0$ is presented as is the one that will be proposed to obtain the far-field irradiance distributions of interest. Other radial orders could be considered, however, given the nature of the PDF of the pointing jitter, the various null rings in between bright irradiance rings of higher-order modes will not in principle be that interesting. Furthermore, the higher the radial mode the higher the beam divergence, and this could limit their application to the problem on hands [52,53].

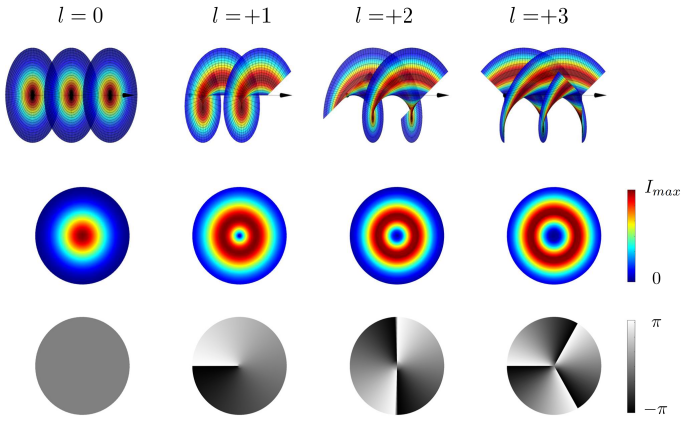

Fig. 4. Laguerre-Gaussian modes of order $l = 0, +1, +2, +3$ and radial order $p = 0$. The first row represents irradiance and phase, the second row represents the irradiance field and the third row is the phase field.

As it has been explained above, under the stochastic behavior of the pointing jitter, the power received in the optical communication terminal will be characterized by the PDF of the power. The analytical approximation obtained for the Gaussian beam for different scenarios (Eqs. (8),(9),(11),(12),(13)), can not be in general expanded to the combination of various orthogonally polarized Laguerre-Gaussian modes. Hence, to obtain the PDF of the power received when far-field irradiance fields described by Eq. (15) are used, the power as a function of the radial displacement of the center can be obtained with Eq. (1). Then, using numerically evaluating Eq. (5), the PDF of the power can be obtained for Rayleigh and Rice distributions with Eqs. (7) and (10), respectively (see Supplement 1 for more details).

2.2. Communication performance

In the previous section, both analytical (only for Gaussian beams) and numerical models have been presented to evaluate the PDF of the power received in an intersatellite link. In this section, the validity of this PDF as a parameter in intersatellite links is justified, and the effect of this PDF on several communication performance parameters is presented.

The transmitter pointing jitter will, at a given instant of time, reduce the power captured by the receiver aperture. The time scale of this fluctuation of power is of uttermost importance when the communication performance is to be evaluated. In a slow fading channel, the variation of the power due to the fading is very slow (its characteristic time is high) compared to the modulation frequency of the communication link. Indeed, this is the case for the intersatellite scenario investigated where the pointing jitter power spectral densities fade away in the ~kHz domain compared to the MHz or GHz frequencies that are typically used to modulate the signal

Optics EXPRESS

in communication links [10]. This type of channel allows us to compute the effect of the power fluctuations due to the transmitter pointing jitter with the slow fading channel model.

First of all, an important parameter in any communication link is the average bit error probability (ABEP). In this paper, on-off keying intensity modulation direct detection (OOK IM/DD) technique is considered. Direct detection systems are widely used because of their much simpler implementation (as they do not need a local oscillator). Furthermore, the far-field irradiance in the proposed optical system is generated by combining two orthogonally polarized beams. Hence, in coherent detection systems in which the incoming beam and the local oscillator have to be of the same polarization, the application of these beams would not be as direct. Finally, from the modulation techniques available in direct detection systems, OOK is the one that can be more efficient if an adaptive optimum threshold is applied [54]. The general expression for ABEP is [16]

$$\text{ABEP} = \int_0^\infty \text{BEP}(h)\, f_{\mathcal{P}}(h)\, dh \tag{20}$$

where the instantaneous conditioned bit error probability for OOK IM/DD is

$$\text{BEP}(h) = Q^G\left(\sqrt{\text{SNR}}\right) \tag{21}$$

where $Q^G(x)$ is the Gaussian Q-function and the signal-to-noise ratio (SNR) is given by

$$\text{SNR} = \frac{2\,(hP_tR)^2}{\sigma_n^2} \tag{22}$$

In Eq. (22), $h = P/P_t$ is the received power normalized by the average transmitted power, P_t is the average transmitted optical power, R is the responsivity of the detector, and σ_n^2 is the signal independent additive white-Gaussian thermal noise.

Furthermore, another important parameter to be evaluated in a communication link is the outage probability. The outage probability is defined as the probability of the instantaneous channel capacity being lower than the rate at which the link is trying to communicate. When this event occurs, the transmitted codewords can no longer be reliably decoded at the receiver side. The outage probability is an important parameter in slow fading channels as the one considered here. This is because, in slow-fading channels, many bits are affected by the fluctuating power losses, as the period of these power fluctuations is orders of magnitude higher than the bit duration. The general expression for outage probability is given by

$$P_{\text{out}}(D_0) = \text{Prob}\left[C(\text{SNR}(h)<D_0\right] \tag{23}$$

where D_0 is the rate at which the link is designed to communicate in [bits/channel use] and C is the capacity of the channel. For a slow-fading, OOK IM/DD modulation, and complete channel state information on the receiver, the instantaneous capacity is written as [11]

$$C(\text{SNR}(h)) = \int \sum_x f_{y|x}(y|x)p_x(x)\log_2\frac{f_{y|x}(y|x)}{f_y(y)}dy \tag{24}$$

where

$$x \in \{0, 2P_t\}$$

$$p_x(x=0) = p_x(x=2P_t) = 0.5$$

$$f_{y|x}(y|x) = \mathcal{N}(hRx, \sigma_n^2)$$

$$f_y(y) = \sum_x p_x(x) f_{y|x}(y|x)$$

where x is the transmitted power and $y = hRx$ is the corresponding electrical signal at the receiver for a detector responsivity given by R. p_x is the probability associated with each x, and $f_{y|x}(y|x)$ is

Optics EXPRESS

the conditional probability characterized by a Gaussian noise $\mathcal{N}(\mu, \sigma_n^2)$ with mean μ and variance σ_n^2. Finally, $f_y(y)$ is the marginal probability for the values of y. The condition given by Eq. (24) can also be converted to

$$P_{\text{out}}(D_0) = \text{Prob}\,[h<h_0] \qquad \text{with} \quad h_0 = \sqrt{\frac{C^{-1}(D_0)\sigma_n^2}{2P_t^2R^2}} \tag{25}$$

where h_0 is the normalized power threshold below which the outage event will occur (see Fig. 3(d)). With Eqs. (20) and (25) the ABEP and the outage probability can be obtained for an intersatellite OOK IM/DD link given the PDF of the power received. Hence, combining the expressions from this subsection and subsection 2.1, the communication performance can be obtained for any far-field irradiance distribution under transmitter pointing jitter perturbations.

3. Optical system design

In the previous section, the mathematical models to compute the ABEP and outage probability for a given far-field irradiance distribution and a pointing jitter PDF have been presented. Our goal is to find an optimum far-field irradiance distribution that maximizes the communication performance of an intersatellite link by minimizing either of these communication performance parameters. In this section, an optical setup that can generate these types of far-field distributions using linearly orthogonally polarized Laguerre-Gaussian beams is presented.

However, when finding an optimum far-field irradiance distribution to minimize either the ABEP or the outage probability in an intersatellite communication link, there are physical limitations that must be taken into account. The problem of finding the far-field irradiance distribution that gives the minimum ABEP or the minimum P_{out} is highly degenerate (meaning that it has many solutions) if the limits imposed by physics are not considered. This means that there can be many far-field irradiance distributions that yield the same ABEP or outage probability. This can be understood directly in the P_{out} case: two far-field irradiance distributions that yield the same cumulative density function of the power for the value h_0 given by Eq. (25) (see Fig. 3(d)), will give the same P_{out}. Therefore, the mathematical problem of finding the optimum far-field without considering any more restrictions is out of the scope of this paper. However, there are certain limits when we consider the physics of wave propagation and the stable far-field electromagnetic fields allowed by this. Indeed, we are looking for a solution that has the following main characteristics:

1. It has to be a stable far-field solution. Stable here means that the far-field irradiance has to change smoothly with distance from the transmitter. For example, top-hat beams that have been considered in other applications [55], i.e., laser welding, are not stable solutions as they will rapidly decay in all kinds of patterns that are different from the top-hat out of the focal region.

2. It has to be simple to generate. To assure a reasonable practical implementation of such a far-field distribution, there should be a simple optical system that can be put onboard a satellite terminal. Indeed, the simplicity will favor lower losses in the transmitter. If the complexity of the system to generate such far-field irradiance distribution is too high, and it involves many optical components, the losses incurred in this system would need to be more than compensated by the resulting far-field distribution gains.

The use of pure or approximate Gaussian beams in free-space optical communications has been thoroughly investigated in previous works [21,24,56,57]. So far, only the adjustment of the divergence of the Gaussian beam has been proposed to mitigate the effects under a given transmitter pointing jitter [11,15,16,18]. In this paper, the use of superposed orthogonally

Optics EXPRESS

polarized higher-order Laguerre-Gaussian beams is investigated to generate a better far-field distribution than in the fundamental Gaussian beam case. These beams will comply with the two requirements imposed above as it will be explained in detail in this section.

To generate a far-field irradiance profile that is given by a superposition of the irradiance fields of two Laguerre-Gaussian modes, the two modes involved should not interfere (see Eq. (15)). In this paper, the latter is attained by using orthogonal polarization states for each of the beams. Figure 5 shows an optical setup that combines two orthogonally polarized beams to generate different far-field irradiance distributions. The linearly polarized Gaussian fundamental beam from the laser source is collimated by the collimating lens. The Rotatable Half-Wave Plate (RHWP) can be used to determine the direction of the linear polarization for the fundamental Gaussian beam entering the polarization beam splitter. On the one hand, if the polarization state after the RHWP is vertical then all the beam will be reflected in the Polarization Beam Splitter (PBS) and will travel to the mirror M1. On the other hand, when the outcoming beam from the RHWP is horizontally polarized the beam will go straight through the PBS and reach mirror M2. For intermediate polarization states the beam will be split in the PBS. Therefore, by rotating the fast axis of the RHWP we can adjust the amount of energy that travels through each of the paths. The fundamental Gaussian beam traveling to mirror M1 will be transmitted by the Spiral Phase Plate (SPP), transforming it into a higher-order Laguerre-Gaussian beam. A SPP is a plate with a helical surface that creates a corresponding spatial phase delay on the beam [58–63] (see upper left side in Fig. 5). The SPP is used to generate the higher-order Laguerre-Gaussian beam due to its polarization-maintaining property (indeed, in this case, the polarization remains vertical) [64]. The helical surface of the SPP is built such that the total height jump s_{SPP} of this is given by

$$s_{\mathrm{SPP}} = \frac{\lambda\, l}{n_{\mathrm{SPP}} - 1} \tag{26}$$

where λ is the wavelength, l is the azimuthal order of the generated Laguerre-Gaussian mode and n_{SPP} is the refraction index of the SPP material. Later on in the optical relay, the horizontally polarized fundamental Gaussian beam is reflected on mirror M2 and combined with the higher-order vertically polarized Laguerre-Gaussian beam in the final polarization beam combiner. The resulting beam is then directed to the telescope of the transmitter terminal and sent towards the receiver. In this setup, the modulation of the laser beam has not been included. For this paper, it is considered that the laser has already been modulated in intensity for communication purposes before entering the optical setup proposed.

The proposed optical system and the resulting communication channel have several limitations when it comes to the detection system, multiplexing techniques, and modulation techniques that can be used. Due to the use of two orthogonally polarized states, the resulting far-field will have a non-uniform linear polarization. Due to these spatial position-dependent polarization states, the use of coherent detection is not trivial for the proposed system. Indeed, coherent detection systems use the interference between the incoming light and a local oscillator onboard the receiver. To create this interference, the polarization state of these two beams has to be the same. As the polarization of the incoming beam to the receiver has both horizontally polarized and vertically polarized components that are dependent on the position, with different pointing errors of the transmitter we will obtain different incoming polarization states (see ellipses in Figs. 5, 13 and 14). A way to partially compensate for these changes would be a polarization state locker that changes to ensure that the polarization of the local oscillator and the incoming beam remains the same [65]. However, this is out of the scope of the current paper and has to be further investigated. On the other hand, a direct detection system will detect the incoming beam power directly without caring for the polarization state of the beam, hence the proposed system is fully compatible with this kind of detection system.

Concerning the multiplexing and modulation techniques, polarization multiplexing and polarization modulation can not be used because this property of light is already being exploited

Optics EXPRESS

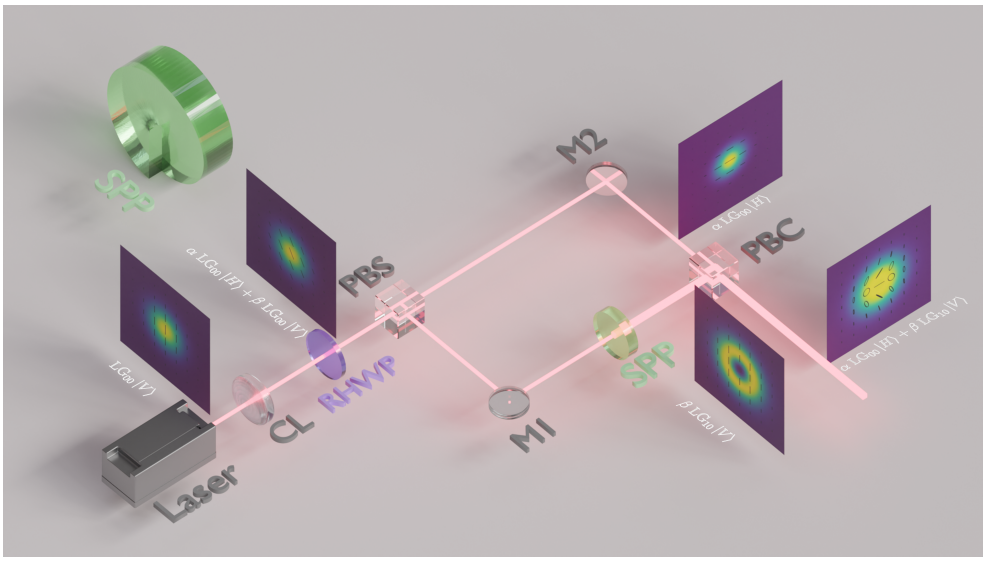

Fig. 5. Optical setup to generate the far-field irradiance distributions of interest. Collimating lens (CL), Rotatable Half-Wave Plate (RHWP), polarization beam splitter (PBS), mirror 1 (M1), mirror 2 (M2), Spiral Phase Plate (SPP), polarization beam combiner (PBC). In the upper left corner, an SPP is illustrated out of scale. $\alpha = a_0$ and $\beta = a_l$ in Eq. (15).

to combine without interference the fundamental Gaussian and the higher order Laguerre-Gaussian beams. Furthermore, spatial division multiplexing or modulation using Laguerre-Gaussian modes can not be used for the same reason. This limitation is not especially relevant for long-range communication links, as spatial division multiplexing or modulation requires that the whole beamwidth is captured by the receiver aperture. Even for small transmitter pointing jitters, the displacement of the transmitted beam from the receiver optical axis in the far field will be too high for capturing a significant section for the space division multiplexed beam.

In Fig. 6 a simulation using Jones calculus and Fourier propagation with gold-protected mirrors in the 1550 nm wavelength is presented for the optical setup proposed in this paper. In this graph, the variation of the power directed through each of the optical branches in the setup (each with either s-polarization or p-polarization) is shown. The losses due to the imperfections of the other elements have not been considered, e.g. the transmission losses and crosstalk in the PBS. It can be seen, that the fraction of power directed through each of the branches, and therefore contributing to either the fundamental Gaussian mode or the higher order Laguerre Gaussian mode, is dependant on the direction of the RHWP's fast axis ψ. The fraction of power P/P_{tot} for $\mathrm{LG}_{00}|H\rangle$ and $\mathrm{LG}_{l0}|V\rangle$ plotted in Fig. 6, corresponds to the weights a_0 and a_l in Eq. (15). Therefore, the optical system proposed in Fig. 5 allows us to tune the far-field irradiance as aimed.

As explained above, this paper proposes two orthogonally polarized states to avoid a variation of the irradiance due to interference between the fundamental and the higher-order Gaussian beam. However, other properties of light can be exploited for the purpose of non-interference. Indeed, two sufficiently separated wavelengths coming from different sources could be used. Analogous to what is proposed with two orthogonally polarized states in Fig. 5, each of the different beams with respective wavelengths would travel different paths giving rise to a multispectral far field. However, there would be several drawbacks related to this kind of setup. Firstly, several laser sources would need to be used and modulated simultaneously. Furthermore, different wavelengths are used usually to separate the different lasers (receiving the beacon, calibration laser, and

Optics EXPRESS

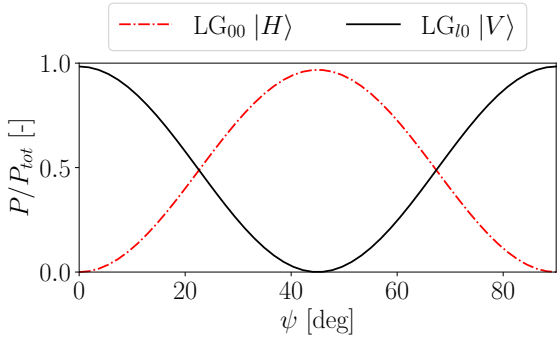

Fig. 6. Variation of the power going through the two branches of the optical setup shown in Fig. 5, as a function of the RHWP fast axis angle w.r.t. the vertical axis, ψ. The light incoming to the RHWP is considered to be vertically polarized (see Fig. 5). The complex index of refraction of the gold-protected mirrors is $n = 0.56 + 9.81i$ and the simulated wavelength is $\lambda = 1550$ nm.

transmitted beacon) traveling through the terminal or to increase the capacity of the channel through wavelength division multiplexing [36,66].

Furthermore, other devices aside from the SPP depicted in Fig. 5 can be used to generate a higher-order Laguerre-Gaussian beam. Several ways have been proposed to generate these types of beams, including the use of spatial light modulators, micromirror arrays, metalenses, and vortex phase plates [67]. The main reasons to use a SPP have been its polarization-maintaining properties and its simplicity and easier implementation for space terminals. Vortex phase plates, generate spatially dependent polarization states of the output higher order beam, and hence this beam would interfere with the fundamental Gaussian beam traveling through the other path. The authors are currently considering metalenses as a potential device to compactly generate the far-field irradiance patterns of interest.

4. Numerical results

The optical design presented in Section 3 can be used to generate the far-field irradiance pattern given by a superposition of the fundamental and a higher-order Laguerre-Gaussian mode. Using different SPPs, the azimuthal order l of the higher-order Laguerre-Gaussian mode can be adjusted. In this paper the results for the combinations $LG_{00} + LG_{10}$, $LG_{00} + LG_{20}$, $LG_{00} + LG_{30}$ and $LG_{00} + LG_{40}$ will be investigated and compared to the fundamental Gaussian beam LG_{00}. With the mathematical model presented in Section 2 the results obtained for the communication performance parameters are presented in this section. To illustrate the intermediate results obtained through the different steps of the model, the reader is referred back to Fig. 3 which illustrates the power statistics and the communication performance obtained for a certain set of parameters for the case $LG_{00} + LG_{10}$. First of all, the far-field irradiance distribution is obtained given the coefficients a_i corresponding to each of the Laguerre-Gaussian modes (see Eq. (15)) and the beamwidth in the receiver aperture plane w_z (Fig. 3(a)). Then, the normalized received power, h, as a function of the pointing error can be computed using the convolution theorem in Eq. (3) (Fig. 3(b)). This is done by computing a bidimensional Fast Fourier Transform. Finally, combining the latter with the PDF of the pointing jitter (Fig. 3(c)), the PDF of the normalized received power, h, is obtained (Fig. 3(d)) using Eq. (5). With this PDF, the ABEP and outage probability can be computed to evaluate the communication performance (Eqs. (20) and (25)). Depending on the receiver telescope design (with on-axis secondary mirror or clear aperture) and the pointing jitter statistics (Rayleigh distribution for non-boresight pointing error and Rice

Optics EXPRESS

distribution for boresighted pointing error), the respective analytical approximations presented in Section 2.1.1 can be used to compute the PDF of the received power for the fundamental Gaussian beam case. For the far-field irradiance pattern given by the superposition of the fundamental and the higher-order Laguerre-Gaussian beam, numerical evaluation of Eqs. (3), (13) and (15) is required as illustrated in Fig. 3.

In an intersatellite link, the distances can vary from the orders of hundreds of kilometers for LEO to LEO optical links, to astronomical distances for deep space optical communications. Furthermore, the transmitter angular pointing jitter, σ_θ can also vary from sub-microradian [27] to tens of milliradians. In this paper, several resulting far-field pointing jitter values are analyzed (see Table 1). The respective relations between the link distance z, and the angular pointing jitter σ_θ can be seen in Fig. 7, for several values of the far-field pointing jitter σ considered in this paper.

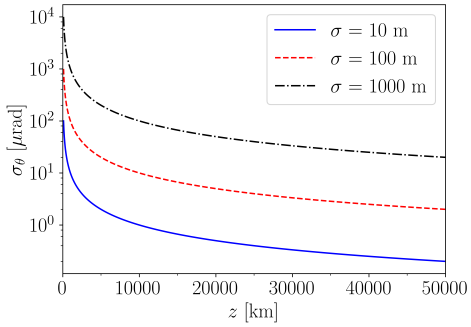

Fig. 7. Relation between the standard deviation of the angular pointing jitter σ_θ and the link distance z for several far-field pointing jitter values σ.

The parameters used for the simulations have been obtained from the literature and are presented in Table 1. In Fig. 8, the values of the ABEP and the outage probability obtained for the optimum combination of LG_{00} and LG_{10} beams can be seen, along with the extreme values obtained using pure LG_{00} ($a_0 = 1$) and LG_{10} ($a_0 = 0$) beams. In these figures, the values for the optimum far-field distribution have been plotted for the respective communication performance parameters. It can be seen that a combination of the fundamental and higher-order Laguerre-Gaussian beams proposed by the authors, yields a better performance of the system compared to the fundamental Gaussian beam, as both the ABEP and the outage probability can be further minimized by using the proposed beams. Furthermore, it can also be seen that the far-field irradiance distribution required to obtain an optimum performance in ABEP is different from the one giving the optimal performance in outage probability. This behavior can also be seen in Fig. 9, where the change as a function of both the beamwidth w_z and the contribution of the fundamental LG_{00} Gaussian beam a_0 is presented, along with the locations of the minima. The same results are plotted in Figs. 10, 11 and 12, when using a combination of the $LG_{00} + LG_{20}$, $LG_{00} + LG_{30}$ and $LG_{00} + LG_{40}$ beams, respectively. From these figures, it can be seen that any of the beams proposed present an improvement with respect to the performance obtained for the fundamental Gaussian beam.

This performance improvement provided by the proposed beams is obtained through the following mechanism: as the transmitter pointing changes, the section of the far-field irradiance that is captured by the receiver aperture changes. The stochastic behavior of the value of h due to these dynamics is captured in the PDF of the normalized received optical power h. Hence, the PDF of h is determined by the far-field irradiance shape as well as the PDF of the pointing jitter (see Fig. 3 and Eq. (5)). Therefore, by changing the far-field irradiance through a superposition of orthogonally polarized Laguerre-Gaussian beams the PDF of h can be changed (Eq. (5)). This

Optics EXPRESS

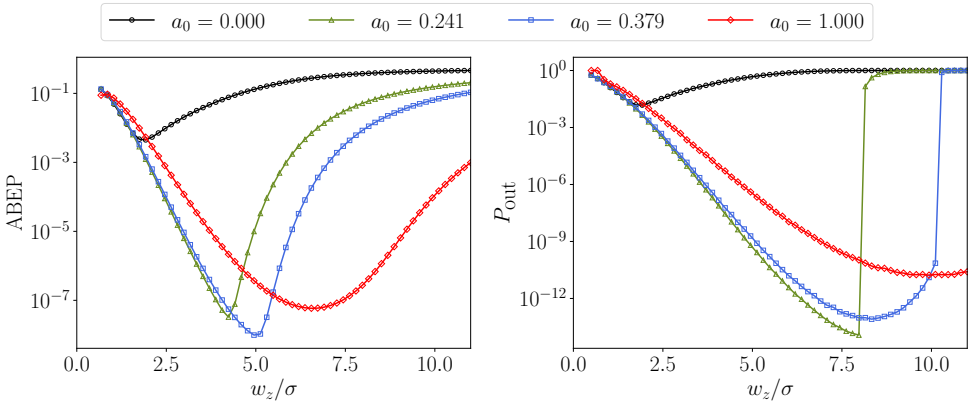

Fig. 8. ABEP and outage probability values for $\sigma = 100$ m and $P_t = 29$ dBm, for different combinations of LG_{00} and LG_{10} modes as a function of w_z. $a_0 = 0.241$ and $a_0 = 0.379$ give the minimum outage probability and ABEP, respectively.

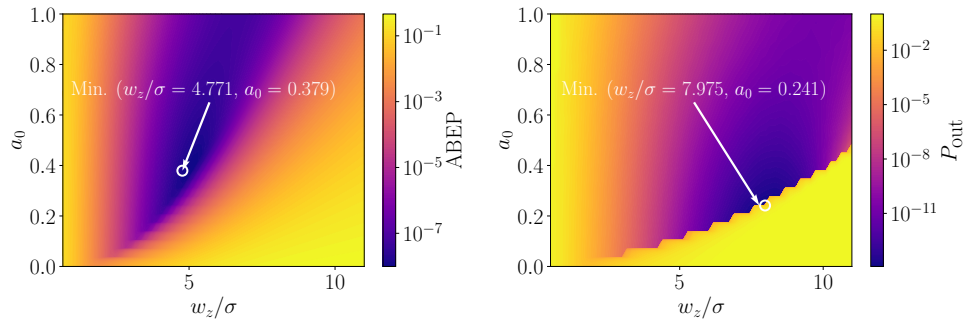

Fig. 9. ABEP and outage probability values for $\sigma = 100$ m and $P_t = 29$ dBm, for LG_{00} and LG_{10} modes as a function of a_0 and w_z.

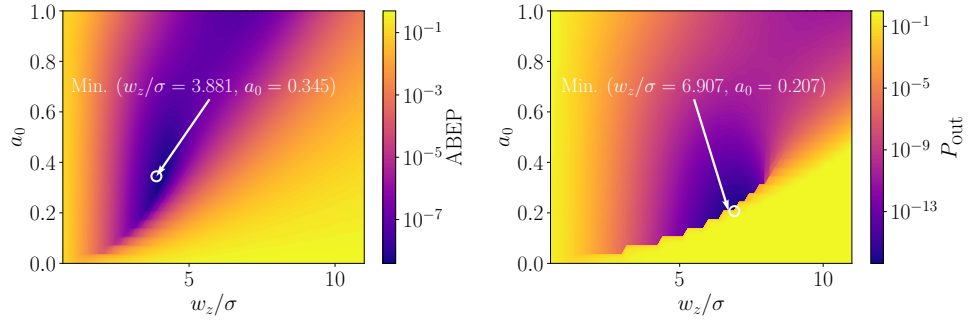

Fig. 10. ABEP and outage probability values for $\sigma = 100$ m and $P_t = 29$ dBm, for different combinations of LG_{00} and LG_{20} modes as a function of w_z.

Optics EXPRESS

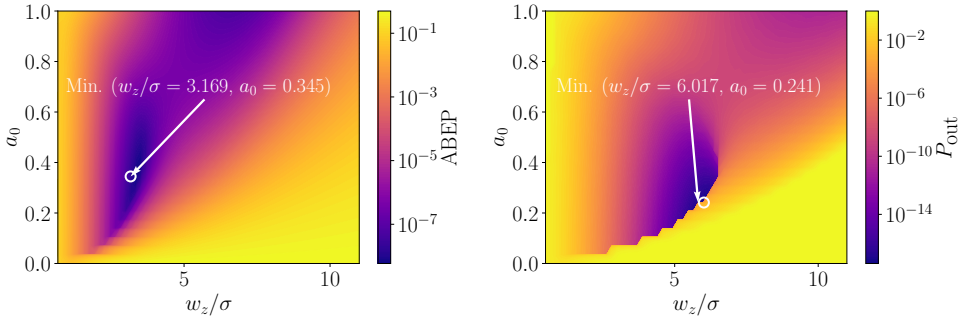

Fig. 11. ABEP and outage probability values for $\sigma = 100$ m and $P_t = 29$ dBm, for different combinations of LG_{00} and LG_{30} modes as a function of w_z.

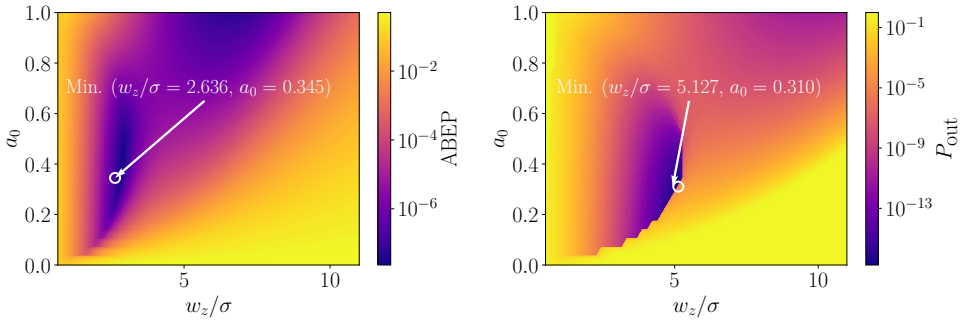

Fig. 12. ABEP and outage probability values for $\sigma = 100$ m and $P_t = 29$ dBm, for different combinations of LG_{00} and LG_{40} modes as a function of w_z.

changes the PDF of the SNR (Eq. (22)), which finally changes the values of ABEP and outage probability (Eqs. (20) and (24)).

The optimum far-field irradiance patterns for obtaining the minimum ABEP are shown in Fig. 13. Each of these far-field irradiance distributions is the one given by the white circle on the left figures of Figs. 9–12. The resulting polarization ellipse of the field in each point is plotted in these figures, as it would be created from the optical setup presented in Section 3. These polarization ellipses are obtained by computing the contribution to the total irradiance by each of the modes, at each point on the receiver aperture plane (see Eq. (15)). Analogously, the optimum far-field irradiance patterns for obtaining the minimum outage probability are shown in Fig. 14 (which correspond to the white circles on the right figures of Figs. 9–12). Several features can be extracted from these figures

1. The optimum far-field irradiance for minimizing ABEP concentrates the power more towards the center receiver optical axis, than the optimum irradiance minimizing for outage probability. This feature can be seen in Figs. 13 and 14. This is true even for the fundamental Gaussian beam LG_{00} (see minima of the red curves in Fig. 8).

2. The higher the order of the Laguerre-Gaussian beam considered, the lower the beamwidth w_z that results in the optimum far-field irradiance for both ABEP and outage probability (see Figs. 9–12).

3. In the analyzed figures, it can be seen that the minima given by the superposition of orthogonally polarized Laguerre-Gaussian beams are more pronounced than the ones given by the fundamental Gaussian beam (see Figs. 8–12). In practice, a system operating in one

Optics EXPRESS

of these minima would have a more sensitive behavior under changes in the beamwidth w_z, compared to the fundamental Gaussian beam. This sensitivity is even more pronounced for the outage probability, when operating in the optimum far-field outage probability (see for example the minimum of the green curve in the right figure of Fig. 8).

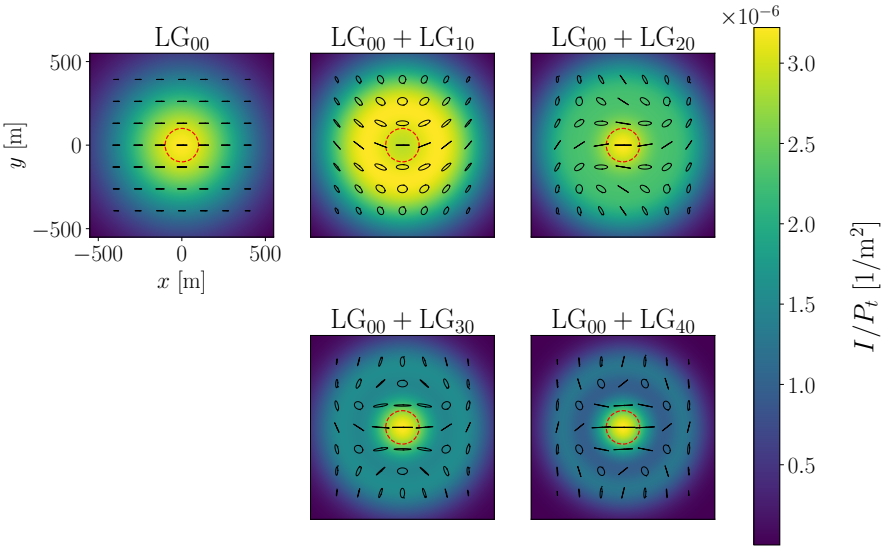

Fig. 13. Far-field irradiance distributions yielding the optimum ABEP. Each figure shows the far-field distribution for the corresponding combination of Laguerre-Gaussian beams, for σ = 100 m and P_t = 29 dBm. The dashed red line shows the magnitude of the pointing jitter scale factor σ. The lines represent the resulting polarization ellipses of the electric field, where the size of the ellipse is proportional to the irradiance at each point. x and y axis are the same for all figures.

To evaluate how much the proposed beams can drive the design of future intersatellite optical terminals, Figs. 15–17 show the minimum ABEP and outage probabilities achievable for different transmitter power values using the beams proposed in this work. Each of the points plotted in these figures refers to the minimum ABEP (or outage probability) that can be obtained by combining orthogonally polarized higher-order Laguerre-Gaussian beams. It can be seen that the power needed to obtain the same ABEP (or outage probability), is lower for orthogonally polarized Laguerre-Gaussian beams than for fundamental Gaussian beams. Furthermore, this trend is confirmed for different magnitudes of the pointing jitter. For σ = 100 m (see Fig. 16) it can be seen also, that up to order l = 2, the higher the azimuthal order of the Laguerre-Gaussian beam, the better the achievable ABEP. However, for l>2, the minimum achievable ABEP starts to increase. Similar behavior can be seen for the outage probability when higher than l = 3 Laguerre-Gaussian beams are considered. It is the authors' opinion that this turning point in performance is due to the increased separation between the central irradiance lobe of the Gaussian fundamental beam and the radial lobe of the higher-order Laguerre-Gaussian beam, as the order of the latter is increased. The radial lobe of low irradiance as the order increases (see bottom figures in Fig. 13 and 14) is frequently captured by the receiver aperture in this case as the pointing jitter is a bivariate Gaussian distribution in the receiver aperture plane. The trend of higher achievable performance with higher azimuthal order l is also limited in practice by the transmitter aperture size. For a given communication distance z the achievable far-field beamwidth w_z is limited by the aperture size of the transmitter. Considering that the transmitted beamwaist w_0 of the beam is located in the aperture plane of the transmitter aperture, the size

Optics EXPRESS

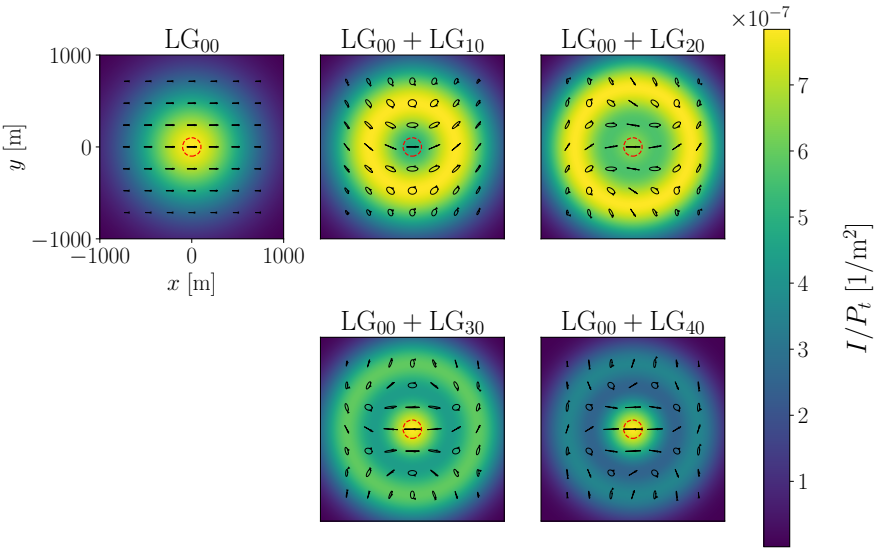

Fig. 14. Far-field irradiance distributions yielding the optimum P_{out}. Each figure shows the far-field distribution for the corresponding combination of Laguerre-Gaussian beams, for $\sigma = 100$ m and $P_t = 29$ dBm. The dashed red line shows the magnitude of the pointing jitter scale factor σ. The lines represent the resulting polarization ellipses of the electric field, where the size of the ellipse is proportional to the irradiance at each point

of the beamwidth in the receiver's aperture plane w_z, is limited by the clipping created in the transmitter's aperture (i.e., the transmitter's aperture size).

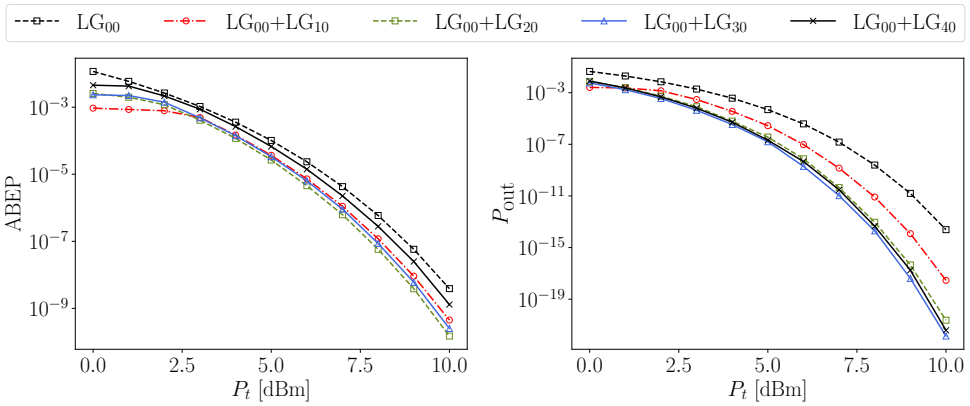

Fig. 15. Optimum ABEP and outage probability as a function of the transmitter power P_t, for $\sigma = 10$ m.

In the analysis presented so far, a pointing jitter given by a Rayleigh distribution and a clear receiver aperture has been considered. On one side, many FSOC intersatellite telescopes have an on-axis secondary mirror [28,29]. The obscuration of the secondary mirror would change the received power statistics and therefore a difference in the results would be expected (see Eq. (2)). However, as the resulting optimum far-field irradiance patterns are in general orders of magnitudes above the aperture size (see Figs. 13 and 14, where the aperture is too small to discern it), the results would be mainly dependant on the total area of the receiver aperture. Hence the

Optics EXPRESS

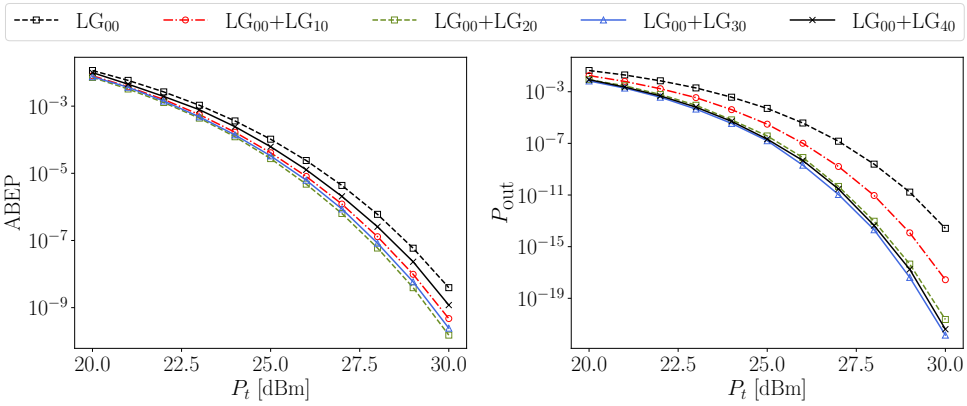

Fig. 16. Optimum ABEP and outage probability as a function of the transmitter power P_t, for $\sigma = 100$ m.

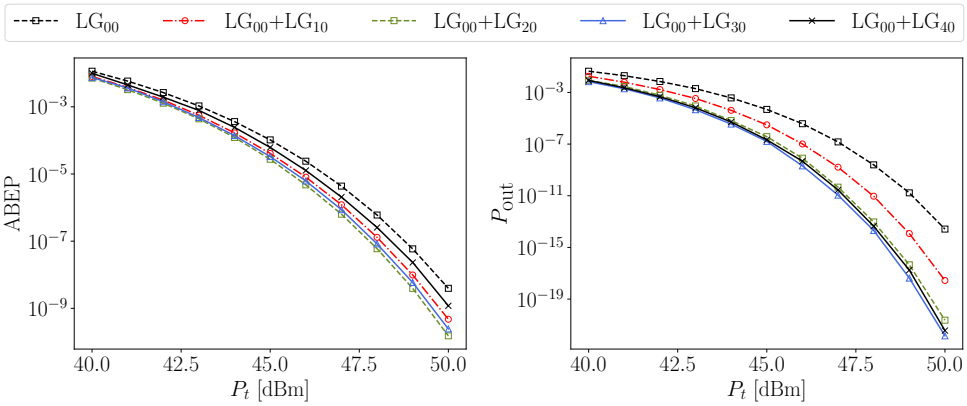

Fig. 17. Optimum ABEP and outage probability as a function of the transmitter power P_t, for $\sigma = 1000$ m.

results shown are also representative of a secondary obscured mirror on the receiver side with an equivalent total aperture area. On the other side, in some links, the pointing jitter will have a static boresight error that will yield a pointing jitter given by a Rice PDF (see Eq. (10)). In this case, if we were to compute the optimum far-field irradiance distributions, a widening of the distribution would be expected. However, if the boresight error is known, the system will usually be calibrated to account for it and the optimization problem will be again one given by the Rayleigh PDF for the pointing jitter.

To quantify the improvement provided by the proposed beams in an intersatellite link scenario, the reduction in the required transmitted power can be analyzed for a 1000km LEO-LEO link. Considering an angular pointing error of $\sigma_\theta = 100$ μrad, the resulting far-field pointing jitter is $\sigma = 100$ m. From Fig. 16 it can be seen that the same ABEP $\approx 10^{-6}$ can be obtained by using $LG_{00} + LG_{20}$ with $\sim 20\%$ less transmitted power, compared to the conventional fundamental Gaussian beam. Similarly, it can be seen in the same figure that a reduction of $\sim 40\%$ required power can be achieved for $LG_{00} + LG_{30}$ when a $P_{\text{out}} \approx 10^{-11}$ is required. For a LEO-GEO link of 45000 km, with the same angular pointing jitter, a far-field pointing jitter of $\sigma = 450$ m would be obtained. As the link is operating somewhere between $\sigma = 100$ m and $\sigma = 1000$ m, and the power savings in both are comparable according to Figs. 16 and 17, power savings

Optics EXPRESS

of the same magnitude would be expected. In summary, these results show that a considerable improvement in intersatellite free space optical communication performance can be obtained by using a superposition of orthogonally polarized fundamental and higher-order Laguerre-Gaussian beams proposed by the authors.

5. Conclusions and future work

In this paper, a superposition of orthogonally polarized fundamental Gaussian and higher-order Laguerre Gaussian beams is proposed to improve the performance of intersatellite free space optical communication links. An optical system to generate the far-field irradiance distributions of interest is presented showing the practical feasibility of generating such far-field irradiance distributions. Finally, numerical results are presented showing transmitted power savings on the order of 20% to 40% that yield the same communication performance as the conventional fundamental Gaussian beams.

There are several topics related to the research presented that need to be further investigated. According to the authors, the most relevant are: (1) the effect of the atmosphere and other factors affecting the quality of the proposed beams, e.g., applicability of the proposed beams in satellite-to-ground or terrestrial links, (2) the generation of the far-field irradiance distributions in a compact way (i.e., metalenses), (3) use of combinations of other beams that are not Laguerre-Gaussian modes, (4) the application to other direct detection modulation techniques such as pulse position modulation and (5) applicability of this research to quantum communication links.

Funding. Nederlandse Organisatie voor Wetenschappelijk Onderzoek (P19-13).

Acknowledgments. The authors would like to thank Rashika Jain, Juan Reto, Joshua Spaander, and Rudolf Saathof for the useful discussions during the process of writing this paper.

Disclosures. The authors declare no conflicts of interest.

Data availability. Data underlying the results presented in this paper are not publicly available at this time but may be obtained from the authors upon reasonable request.

Supplemental document. See Supplement 1 for supporting content.

References

1. H. Hemmati, *Near-Earth Laser Communications* (CRC, 2009).
2. S.-K. Liao, H.-L. Yong, C. Liu, *et al.*, "Long-distance free-space quantum key distribution in daylight towards inter-satellite communication," Nat. Photonics **11**(8), 509–513 (2017).
3. M. Gündogan, J. S. Sidhu, V. Henderson, *et al.*, "Proposal for space-borne quantum memories for global quantum networking," npj Quantum Inf. **7**(1), 128 (2021).
4. S. Khatri, A. J. Brady, R. A. Desporte, *et al.*, "Spooky action at a global distance: analysis of space-based entanglement distribution for the quantum internet," npj Quantum Inf. **7**(1), 4–15 (2021).
5. R. Bedington, J. M. Arrazola, and A. Ling, "Progress in satellite quantum key distribution," npj Quantum Inf. **3**(1), 30 (2017).
6. Z. Sodnik, B. Furch, and H. Lutz, "Optical Intersatellite Communication," IEEE J. Sel. Top. Quantum Electron. **16**(5), 1051–1057 (2010).
7. Y. Horst, B. I. Bitachon, L. Kulmer, *et al.*, "Tbit/s line-rate satellite feeder links enabled by coherent modulation and full-adaptive optics," Light: Sci. Appl. **12**(1), 153 (2023).
8. W. Wang, Y. Zhang, Y. Zhao, *et al.*, "Gravity-based network traffic abstraction and laser ON/OFF control in optical satellite networks," J. Opt. Commun. Netw. **15**(12), 958–968 (2023).
9. L. C. Andrews, R. L. Phillips, and C. Y. Young, "Scintillation model for a satellite communication link at large zenith angles," Opt. Eng. **39**(12), 3272–3280 (2000).
10. M. Badás, P. Piron, J. Bouwmeester, *et al.*, "Opto-thermo-mechanical phenomena in satellite free-space optical communications: survey and challenges," Opt. Eng. **63**(4), 041206 (2023).
11. A. A. Farid and S. Hranilovic, "Outage Capacity Optimization for Free-Space Optical Links With Pointing Errors," J. Lightwave Technol. **25**(7), 1702–1710 (2007).
12. H. G. Sandalidis, T. A. Tsiftsis, and G. K. Karagiannidis, "Optical Wireless Communications With Heterodyne Detection Over Turbulence Channels With Pointing Errors," J. Lightwave Technol. **27**(20), 4440–4445 (2009).
13. F. Yang, J. Cheng, and T. A. Tsiftsis, "Free-Space Optical Communication with Nonzero Boresight Pointing Errors," IEEE Trans. Commun. **62**(2), 713–725 (2014).

Optics EXPRESS

14. C.-C. Chen and C. Gardner, "Impact of random pointing and tracking errors on the design of coherent and incoherent optical intersatellite communication links," IEEE Trans. Commun. **37**(3), 252–260 (1989).
15. M. Toyoshima, T. Jono, K. Nakagawa, *et al.*, "Optimum divergence angle of a Gaussian beam wave in the presence of random jitter in free-space laser communication systems," J. Opt. Soc. Am. A **19**(3), 567–571 (2002).
16. T. Song, Q. Wang, M.-W. Wu, *et al.*, "Impact of Pointing Errors on the Error Performance of Intersatellite Laser Communications," J. Lightwave Technol. **35**(14), 3082–3091 (2017).
17. I. U. Zaman and O. Boyraz, "Impact of receiver architecture on small satellite optical link in the presence of pointing jitter," Appl. Opt. **59**(32), 10177–10184 (2020).
18. P. X. Do, A. Carrasco-Casado, T. V. Vu, *et al.*, "Numerical and analytical approaches to dynamic beam waist optimization for LEO-to-GEO laser communication," OSA Continuum **3**(12), 3508–3522 (2020).
19. S. Huang and M. Safari, "Free-Space Optical Communication Impaired by Angular Fluctuations," IEEE Trans. Wireless Commun. **16**(11), 7475–7487 (2017).
20. X. Jiao, J. Zhang, W. Li, *et al.*, "Advances in spacecraft micro-vibration suppression methods," Prog. Aeronaut. Sci. **138**, 100898 (2023).
21. L. C. Andrews and R. L. Phillips, *Laser Beam Propagation Through Random Media* (SPIE, 2005).
22. J. B. Thomas, *Introduction to Probability* (Springer, 1986).
23. A. Carrasco-Casado, K. Shiratama, D. Kolev, *et al.*, "Development and Space-Qualification of a Miniaturized CubeSat's 2-W EDFA for Space Laser Communications," Electronics **11**(15), 2468 (2022).
24. H. T. Yura, "Optimum truncation of a Gaussian beam in the presence of random jitter," J. Opt. Soc. Am. A **12**(2), 375–379 (1995).
25. R. D. Nelson, T. H. Ebben, and R. G. Marshalek, "Experimental Verification Of The Pointing Error Distribution Of An Optical Intersatellite Link," in *Free-Space Laser Communication Technologies*, vol. 0885 (SPIE, 1988), pp. 132–142.
26. M. Toyoshima, Y. Takayama, H. Kunimori, *et al.*, "In-orbit measurements of spacecraft microvibrations for satellite laser communication links," Opt. Eng. **49**(8), 083604 (2010).
27. X. Wang, X. Wang, C. Li, *et al.*, "Angular micro-vibration of the Micius satellite measured by an optical sensor and the method for its suppression," Appl. Opt. **60**(7), 1881–1887 (2021).
28. C. E. DeVoe, A. D. Pillsbury, F. Khatri, *et al.*, "Optical overview and qualification of the LLCD space terminal," in *International Conference on Space Optics*, vol. 10563 (SPIE, 2017), pp. 115–123.
29. T. Tolker-Nielsen and J.-C. Guillen, "SILEX: The First European Optical Communication Terminal in Orbit," ESA Bulletin **96**, 1 (1998).
30. J. Cheng, *The Principles of Astronomical Telescope Design* (Springer, 2009).
31. M. Toyoshima, N. Takahashi, T. Jono, *et al.*, "Mutual alignment errors due to the variation of wave-front aberrations in a free-space laser communication link," Opt. Express **9**(11), 592–602 (2001).
32. V. S. R. Gudimetla and J. F. Riker, "Moment-matching method for extracting beam jitter and boresight in experiments with satellites of small physical cross section," Appl. Opt. **46**(23), 5608–5616 (2007).
33. M. Toyoshima and K. Araki, "Far-field pattern measurement of an onboard laser transmitter by use of a space-to-ground optical link," Appl. Opt. **37**(10), 1720–1730 (1998).
34. A. Carrasco-Casado, K. Shiratama, D. Kolev, *et al.*, "Prototype Development and Validation of a Beam-Divergence Control System for Free-Space Laser Communications," Front. Phys. **10**, 1 (2022).
35. A. E. Siegman, *Lasers* (University Science Books, 1986).
36. A. E. Willner, K. Zou, K. Pang, *et al.*, "Free-space mid-IR communications using wavelength and mode division multiplexing," Opt. Commun. **541**, 129518 (2023).
37. A. E. Willner, H. Song, K. Zou, *et al.*, "Orbital Angular Momentum Beams for High-capacity Communications," J. Lightwave Technol. **41**(7), 1918–1933 (2023).
38. A. E. Willner and C. Liu, "Perspective on using multiple orbital-angular-momentum beams for enhanced capacity in free-space optical communication links," Nanophotonics **10**(1), 225–233 (2020).
39. A. Willner, H. Zhou, X. Su, *et al.*, "Utilizing Structured Modal Beams in Free-Space Optical Communications for Performance Enhancement," IEEE J. Sel. Top. Quantum Electron. **29**(6: Photonic Signal Processing), 1–13 (2023).
40. X. Zhong, Y. Zhao, G. Ren, *et al.*, "Influence of Finite Apertures on Orthogonality and Completeness of Laguerre-Gaussian Beams," IEEE Access **6**, 8742–8754 (2018).
41. M. J. Padgett, F. M. Miatto, M. P. J. Lavery, *et al.*, "Divergence of an orbital-angular-momentum-carrying beam upon propagation," New J. Phys. **17**(2), 023011 (2015).
42. J. W. Lee, J. Y. Choi, Y. J. Hyun, *et al.*, "Solar background noise mitigation using the orbital angular momentum mode in vertical FSO downlink transmissions," Opt. Express **29**(21), 33312 (2021).
43. A. Trichili, A. B. Salem, A. Dudley, *et al.*, "Encoding information using Laguerre Gaussian modes over free space turbulence media," Opt. Lett. **41**(13), 3086–3089 (2016).
44. L. Zhu, A. Wang, M. Deng, *et al.*, "Free-space optical communication with quasi-ring Airy vortex beam under limited-size receiving aperture and atmospheric turbulence," Opt. Express **29**(20), 32580–32590 (2021).
45. D. Yang, Z. Yu, W. Wang, *et al.*, "Underwater entanglement propagation of auto-focusing Airy beams," Opt. Express **32**(4), 4887 (2024).
46. S. Li and J. Wang, "Adaptive free-space optical communications through turbulence using self-healing Bessel beams," Sci. Rep. **7**(1), 43233 (2017).

Optics EXPRESS

47. S. Shang, J. Zhang, Y. Qi, *et al.*, "Fiber coupling efficiency of a Bessel–Gaussian beam received by a Cassegrain antenna under atmospheric turbulence," Appl. Opt. **61**(23), 6871–6878 (2022).
48. C. Lyu, M. R. Belic, Y. Li, *et al.*, "Generation of diffraction-free Bessel beams based on combined axicons," Opt. Laser Technol. **164**, 109548 (2023).
49. J. Yang, W. Hu, A. Wang, *et al.*, "Generation and free-space transmission characterization of bottle vortex beam," Opt. Express **31**(25), 41094–41104 (2023).
50. F. Saad, H. Benzehoua, and A. Belafhal, "Propagation behavior of a generalized Hermite cosh-gaussian laser beam through marine environment," Opt. Quantum Electron. **56**(1), 130 (2024).
51. N. K. Fontaine, H. Chen, M. Mazur, *et al.*, "Hermite-Gaussian mode multiplexer supporting 1035 modes," in *Optical Fiber Communications Conference and Exhibition* (2021), pp. 1–3.
52. J. Wang, J.-Y. Yang, I. M. Fazal, *et al.*, "Terabit free-space data transmission employing orbital angular momentum multiplexing," Nat. Photonics **6**(7), 488–496 (2012).
53. H. Huang, G. Xie, Y. Yan, *et al.*, "100 Tbit s free-space data link enabled by three-dimensional multiplexing of orbital angular momentum, polarization, and wavelength," Opt. Lett. **39**(2), 197–200 (2014). Publisher: Optica Publishing Group.
54. E. J. Lee and V. W. Chan, "Diversity Coherent and Incoherent Receivers for Free-Space Optical Communication in the Presence and Absence of Interference," J. Opt. Commun. Netw. **1**(5), 463 (2009).
55. F. M. Dickey, S. C. Holswade, and D. M. Shealy, eds., *Laser Beam Shaping Applications* (CRC, 2018).
56. H. Hemmati, A. Biswas, and I. B. Djordjevic, "Deep-Space Optical Communications: Future Perspectives and Applications," Proc. IEEE **99**(11), 2020–2039 (2011).
57. H. Hemmati, *Deep Space Optical Communications* (John Wiley & Sons, 2006).
58. M. Massari, G. Ruffato, M. Gintoli, *et al.*, "Fabrication and characterization of high-quality spiral phase plates for optical applications," Appl. Opt. **54**(13), 4077–4083 (2015).
59. G. Ruffato, M. Carli, M. Massari, *et al.*, "Spiral phase plates for the generation of high-order Laguerre-Gaussian beams with non-zero radial index," in *Complex Light and Optical Forces IX*, vol. 9379 (SPIE, 2015), pp. 11–21.
60. W. Pan, L. Xu, J. Li, *et al.*, "Generation of High-Purity Laguerre–Gaussian Beams by Spatial Filtering," IEEE Photonics J. **11**(3), 1–10 (2019).
61. M. Ca no-García, X. Quintana, J. M. Otón, *et al.*, "Dynamic multilevel spiral phase plate generator," Sci. Rep. **8**(1), 15804 (2018).
62. K. M. Dorney, L. Rego, N. J. Brooks, *et al.*, "Controlling the polarization and vortex charge of attosecond high-harmonic beams via simultaneous spin–orbit momentum conservation," Nat. Photonics **13**(2), 123–130 (2019).
63. K. Toyoda, K. Miyamoto, N. Aoki, *et al.*, "Using Optical Vortex To Control the Chirality of Twisted Metal Nanostructures," Nano Lett. **12**(7), 3645–3649 (2012).
64. J. Sun, J. Zeng, X. Wang, *et al.*, "Concealing with Structured Light," Sci. Rep. **4**(1), 4093 (2014).
65. J. E. Nordholt, R. T. Newell, C. G. Peterson, *et al.*, "Polarization tracking system for free-space optical communication, including quantum communication," Tech. Rep. 9,866,379, Los Alamos National Laboratory (LANL), Los Alamos, NM (United States) (2018).
66. W. Shao, Y. Wang, S. Jia, *et al.*, "Terabit FSO communication based on a soliton microcomb," Photonics Res. **10**(12), 2802–2808 (2022).
67. Y. Lian, X. Qi, Y. Wang, *et al.*, "OAM beam generation in space and its applications: A review," Opt. Lasers Eng. **151**, 106923 (2022).